

Solar Wind Helium Abundance Heralds Solar Cycle Onset

Benjamin L. Alterman^{1,2}  · Justin C. Kasper^{3,2}  · Robert J. Leamon^{4,5}  · Scott W. McIntosh⁶ 

© Springer ●●●

Abstract

We study the solar wind helium-to-hydrogen abundance's (A_{He}) relationship to solar cycle onset. Using OMNI/Lo data, we show that A_{He} increases prior to sunspot number (SSN) minima. We also identify a rapid depletion and recovery in A_{He} that occurs directly prior to cycle onset. This A_{He} Shutoff happens at approximately the same time across solar wind speeds (v_{sw}), implying that it is formed by a mechanism distinct from the one that drives A_{He} 's solar cycle scale variation and v_{sw} -dependent phase offset with respect to SSN. The time between successive A_{He} shutoffs is typically on the order of the corresponding solar cycle length. Using Brightpoint (BP) measurements to provide context, we

✉ B.L. Alterman
blalterman@swri.org
J.C. Kasper
jckasper@umich.edu
R.J. Leamon
robert.j.leamon@nasa.gov
S.W. McIntosh
mscott@ucar.edu

- ¹ Space Science and Engineering, Southwest Research Institute, 6220 Culebra Road, San Antonio, TX 78238, USA
- ² University of Michigan, Department of Climate & Space Sciences & Engineering, 2455 Hayward St., Ann Arbor, MI 48109-2143, USA
- ³ BWX Technologies, Inc. Washington, D.C. 20002, USA
- ⁴ University of Maryland–Baltimore County, Goddard Planetary Heliophysics Institute, Baltimore, MD 21250, USA
- ⁵ NASA Goddard Space Flight Center, Code 672, Greenbelt, MD 20771, USA
- ⁶ National Center for Atmospheric Research, High Altitude Observatory, P.O. Box 3000, Boulder, CO 80307, USA

infer that this shutoff is likely related to the overlap of adjacent solar cycles and the equatorial flux cancelation of the older, extended solar cycle during Solar Minima.

Keywords: Solar Cycle, Observations – Solar Wind – Sunspots

1. Introduction

Since at least 1844, the Sun’s approximately 11-year solar activity cycle has been measured in the sunspot number (SSN) (Schwabe, 1844). Today, many other activity indices are known to track the solar cycle. Typically, these carry a known phase offset when measured with respect to SSN. For example, Lyman- α ($L\alpha$) lags SSN by 125 days (Bachmann and White, 1994) and soft X-ray flux (SXR) lags SSN by 300 to 450 days (Temmer, Veronig, and Hanslmeier, 2003).

Helium is a natural byproduct of Big Bang nucleosynthesis and solar fusion (Bethe and Critchfield, 1938; Bethe, 1939; Parker, 1997; Basu and Antia, 2008). It composes $\sim 25\%$ of solar material by mass (Basu and Antia, 2008; Asplund *et al.*, 2009; Laming, 2015; Basu and Antia, 2004) and is the most common solar element after hydrogen. The first ionization potential (FIP) is the energy necessary to ionize a neutral atom’s 1st electron. As helium has the highest FIP of any solar element, it is the last to ionize in the upper convection zone (Basu and Antia, 2008; Laming, 2015). Through the chromosphere and transition region, the FIP effect depletes the helium abundance (Laming, 2015; Rakowski and Laming, 2012) such that, outside of transient events like coronal mass ejections (CMEs), it drops to below 5% by the time its is released into the solar wind (Asplund *et al.*, 2009; Laming, 2015; Hirshberg, 1973; Neugebauer, 1981; Aellig, Lazarus, and Steinberg, 2001; Kasper *et al.*, 2007, 2012; Alterman and Kasper, 2019).

Neugebauer and Snyder (1962) made the first in situ helium measurements with Mariner II. The helium abundance is given by

$$A_{\text{He}} = 100 \times n_{\text{He}}/n_{\text{H}}, \quad (1)$$

where n_{He} is the helium number density and n_{H} is the hydrogen number density. In the intervening 58 years, multiple authors have shown that A_{He} tracks the solar cycle (Ogilvie and Hirshberg, 1974; Feldman *et al.*, 1978; Ogilvie *et al.*, 1989; Aellig, Lazarus, and Steinberg, 2001; McIntosh *et al.*, 2011; Kasper *et al.*, 2007, 2012; Zerbo and Richardson, 2015; Alterman and Kasper, 2019). In particular, A_{He} ’s response lags changes in SSN (Feldman *et al.*, 1978) and this lag monotonically increases with v_{sw} (Alterman and Kasper, 2019).

Brightpoints (BPs) are localized enhancements at extreme ultraviolet (EUV) (McIntosh, 2007), x-ray (Vaiana, Krieger, and Timothy, 1973), or both wavelengths. BPs are a key solar activity indicator and, “represent a set of low-corona small-scale loops with enhanced emission in the extreme-ultraviolet and X-ray spectrum that connect magnetic flux concentrations of opposite polarities.” (Madjarska, 2019) McIntosh (2007) determined that EUV BPs are likely rooted at the vertices of supergranule cells and the flow of the supergranules in which

they are anchored drives them. As BPs are signatures of solar activity, it is perhaps unsurprising that their occurrence follows the butterfly pattern (McIntosh *et al.*, 2014a; Leamon, Chapman, and Watkins, 2020), which Spörer’s Law (Maunder, 1903) associates with sunspots (Carrington, 1863).

In this Article, we continue the process of connecting solar wind A_{He} to the solar activity cycle. Section 2 describes our data sources and selection. Section 3 extends observations of A_{He} ’s variation with solar cycle to cover a 45 year period from 1974 until present day. Here, we present two as-yet undiscussed observations.

- i) Immediately prior to Solar Minima, A_{He} rapidly depletes and then recovers over $\lesssim 250$ days at all solar wind speeds. We refer to this as A_{He} or Helium Shutoff.
- ii) The time between these rapid A_{He} shutoffs is approximately the same as the time between successive SSN minima.

Section 4 contextualizes A_{He} Shutoffs prior to Solar Minima with EUV BPs. This connection relates A_{He} ’s rapid depletions or shutoffs with the time period when two solar cycles overlap and the equatorial bands of the Sun’s toroidal field related to the older, decaying extended cycle cancel. Section 5 discusses our results. Section 6 briefly concludes.

2. Data Sources and Selection

This study combines in situ OMNI plasma measurements with *Solar Dynamics Observatory* (SDO) and *Solar and Heliospheric Observatory* (SOHO) remote observations. Several solar activity indices provide context.

The OMNI database¹ contains solar wind magnetic field, thermal plasma, and energetic proton measurements at multiple high² and low³ time resolutions (King and Papitashvili, 2005). These measurements are collected from multiple spacecraft, both near-Earth and at the 1st Lagrange point (L1). This study uses near-Earth Low Resolution OMNI (OMNI/Lo) data. The L1-collected data is propagated to, “expected magnetosphere-arrival times,” (https://omniweb.gsfc.nasa.gov/html/ow_data.html) and then averaged to 1 hour cadence. While OMNI/Lo data begins in 1963 and extends to the present day, we limit this study to data collected beginning in 1974.

The *Wind* Solar Wind Experiment (SWE) Faraday Cups (FCs) are the primary source of present day OMNI/Lo data.⁴ Multiple SWE/FC data products are available (Ogilvie *et al.*, 1995; Kasper *et al.*, 2006; Maruca and Kasper, 2013; Alterman *et al.*, 2018). Per documentation⁵, all data are cross-normalized

¹<https://omniweb.gsfc.nasa.gov/>

²5 minute and 1 minute (https://omniweb.gsfc.nasa.gov/html/omni_min_data.html)

³1 hour and longer (https://omniweb.sci.gsfc.nasa.gov/html/ow_data.html)

⁴https://omniweb.gsfc.nasa.gov/html/ow_data.html

⁵Ibid.

to the SWE/FC data derived according to Kasper *et al.* (2006). Since this study focuses on the steady state solar wind and not transients such as coronal mass ejections (CMEs), we require that OMNI/Lo data satisfy $A_{\text{He}} \leq 15\%$ and $v_{\text{sw}} < 1000 \text{ km s}^{-1}$. Prior work has shown that more detailed removal of transients such as CMEs do not significantly change the average A_{He} (Kasper *et al.*, 2007). We access the OMNI data using FTP protocols via the *heliopy* (Stansby *et al.*, 2020) software library.

The *Solar and Heliospheric Observatory* (SOHO) *Extreme-ultraviolet Imaging Telescope* (EIT) (Delaboudinière *et al.*, 1995) and *Solar Dynamics Observatory* (SDO) *Atmospheric Imaging Assembly* (AIA) (Lemen *et al.*, 2012) telescopes provide our EUV measurements at 195Å and 193Å, respectively. Following McIntosh *et al.* (2014a), we identify BPs in a manner that accounts for differences in the two instruments. We make no distinction between quiet Sun and active region (AR) BPs; calculate a daily average of those lying along the central meridian; and then average the daily BP measurements down to 27-day cadence.

We use three solar activity indicators to provide solar cycle context. The Solar Information Data Center (SILSO World Data Center, 2020; Vanlommel *et al.*, 2005, SIDC) provides our SSN data. LASP’s Interactive Solar Irradiance Data Center (Leise *et al.*, 2019, LISIRD) provides F10.7 cm radio emission and Lyman- α ($L\alpha$) data, which demonstrate a response that lags Solar Minima.

3. Heralding the Solar Cycle

Figure 1 Panel (A, top) plots the OMNI/Lo A_{He} as a function of v_{sw} and time. v_{sw} has been split into 12 quantiles over the entire mission and A_{He} within each quantile is averaged down to 250-day time resolution. Following Alterman and Kasper (2019) and Kasper *et al.* (2007, 2012), the slowest quantile is at the edge of any given instruments operational capabilities and the fastest covers several hundred km s^{-1} . As such, these two quantiles are excluded and Figure 1 covers the v_{sw} range 319 km s^{-1} to 602 km s^{-1} , i.e. slow and intermediate speed solar wind. The legend indicates the middle of each quantile in km s^{-1} . Error bars indicate the standard error of the mean. Starting in ~ 1985 , each error bar is smaller than the corresponding marker.

Figure 1 provides solar cycle context with three activity indices. The 13 month smoothed SSN (--) is plotted against Panel (A)’s secondary y-axis. By convention, each numbered solar cycle is defined from one Sunspot Minimum to the following Minimum. Purple dash-dotted lines (---) identify established Solar Minima⁶ and the recently announced Solar Minimum 25 during December 2019^{7,8}, each labeled in a gray bar at Panel (B)’s bottom. Panel (B, bottom) plots $L\alpha$ (left, solid blue, —) and F10.7 cm radio emission (right, dashed orange, ---). To match SSN data, both have been averaged to monthly cadence and then

⁶sidc.oma.be/silso/DATA/Cycles/TableCyclesMiMa.txt

⁷sidc.be/silso/node/167/#NewSolarActivity

⁸nasa.gov/press-release/solar-cycle-25-is-here-nasa-noaa-scientists-explain-what-that-means

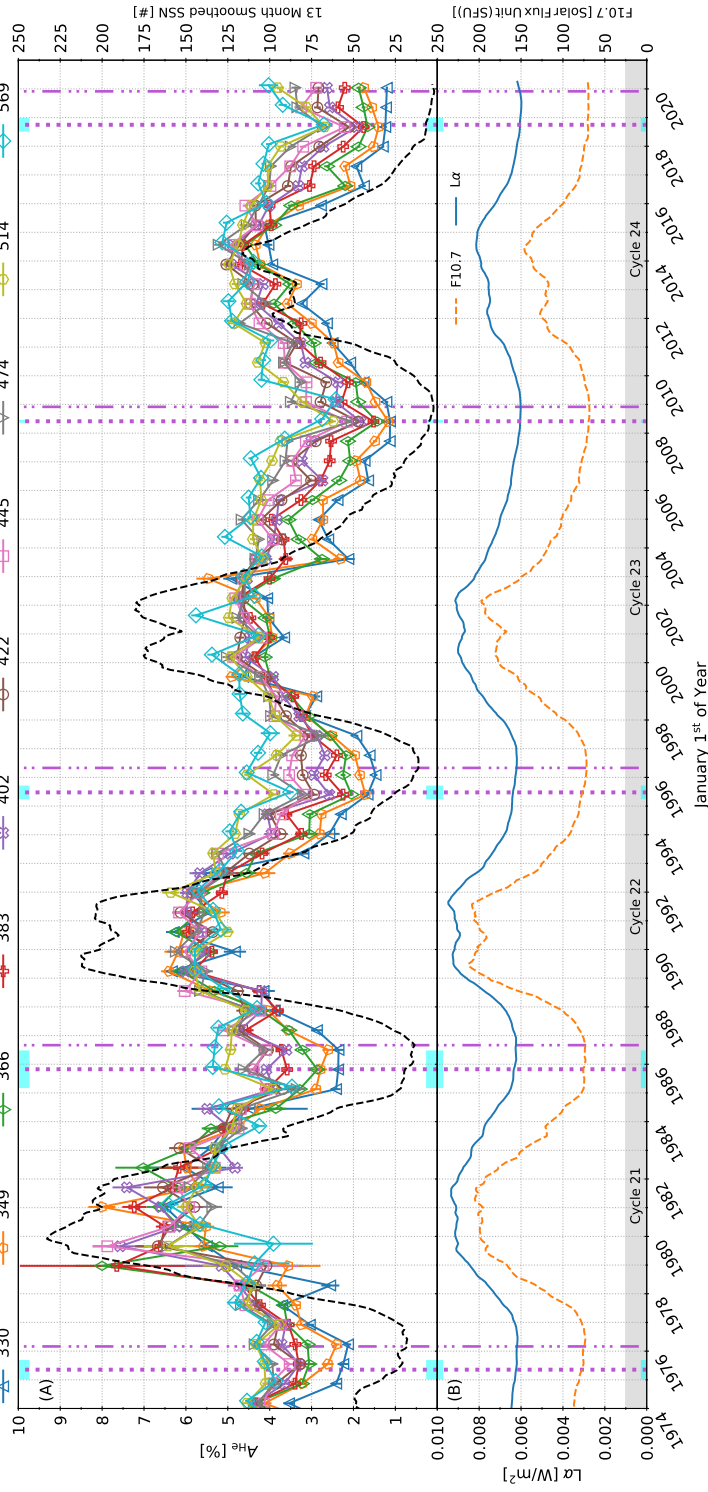


Figure 1. (A) OMNI/Lo helium abundance (A_{He}) as a function of solar wind speed (v_{sw}) and time. A_{He} is split into 10 v_{sw} -quantile, each indicated by a unique color and marker. The legend at the figure's top indicates each quantile's center in km s^{-1} . Within each v_{sw} -quantile, A_{He} is averaged down to 250-day resolution. Error bars indicate the standard error of the mean. The secondary y-axis plots the 13 month smoothed sunspot number (SSN, --). Vertical dash-dotted purple lines (---) indicate Solar Cycle Minima, which conventionally indicate the start of a new solar cycle. Vertical dotted lines (···) indicate the A_{He} Shutoff date averaged across v_{sw} -quantiles. Blue boxes (■) at the top and bottom of each panel indicate the standard deviation of these shutoff dates. **(B)** Lyman- α ($L\alpha$, left, -) and F10.7 cm radio emission (right, --) solar activity indicators over the same period as A_{He} . Within one or two data points, A_{He} increases across all but the one or two slowest v_{sw} -quantiles prior to plotted SSN Minima.

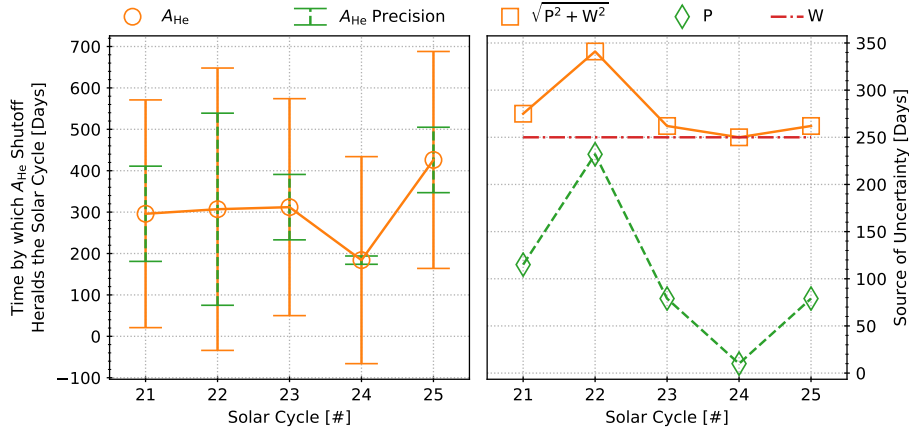


Figure 2. (Left) Orange circles (\circ) plot the time by which A_{He} Shutoff heralds a given solar cycle. Green error bars ($-$) indicate the uncertainty only due to A_{He} 's precision (P). Orange error bars ($-$) show the uncertainty due to the geometric mean of the precision and the 250-day averaging window length ($\sqrt{P^2 + W^2}$). (Right) Sources of uncertainty in each of the (Left) panel's data points. Orange diamonds (\diamond) and green squares (\square) plot the uncertainties indicated in the same color that the (Left) panel uses. The red dash-dotted line ($-$) indicates the 250-day averaging window (W). The 250-day averaging window is the dominant source of uncertainty in determining when A_{He} Shutoff occurs.

smoothed with a centered 13 month window. Visual inspection shows that both $L\alpha$ and F10.7 reach a minimum after SSN.

As Alterman and Kasper (2019) observe directly with *Wind*/SWE data, OMNI/Lo A_{He} reached a consistent maximum during cycles 23 and 24 of $4\% \lesssim A_{\text{He}} \lesssim 5\%$ across v_{sw} quantiles. Cycle 24's Minimum and declining phase also indicate that the helium abundance has reached a similar value bottoming out at $\sim 1\%$ in the slowest speeds. Extrema 21 and 22 show similar, mutually consistent behavior. A_{He} during these Minima bottom out at $\sim 2\%$ and these maxima peak between $5\% \lesssim A_{\text{He}} \lesssim 6\%$. Minimum 23 bottoms out at a value intermediate between the prior and following Solar Minima. A_{He} may also carry signatures of the double peak or Gnevyshev gap (Hathaway, 2015, double SSN peaks) across all Sunspot Maxima, which is the study of future work.

Alterman and Kasper (2019) observed a decline in A_{He} during cycle 24's trailing edge. Figure 1 shows that—on this 250-day timescale— A_{He} has reached a local minimum and is now ascending towards is Solar Maximum values across all but the slowest v_{sw} -quantile. Figure 1 also indicates an as-yet undiscussed feature across multiple Solar Minima: on the 250-day timescale used here, **a sharp departure from A_{He} 's local sinusoidal trend appears in all but the slowest one or two v_{sw} -quantiles before Solar Minima 22 through 25**. Vertical dotted lines (\cdots) indicate the date of these rapid A_{He} depletions or shutoffs, averaged across v_{sw} -quantiles. The blue bands (\blacksquare) on the top and bottom of each panel surrounding the dotted lines are the associated standard deviation of the dates. These two features demonstrate that A_{He} **shutoff occurs prior to Solar Minima as defined by SSN**.

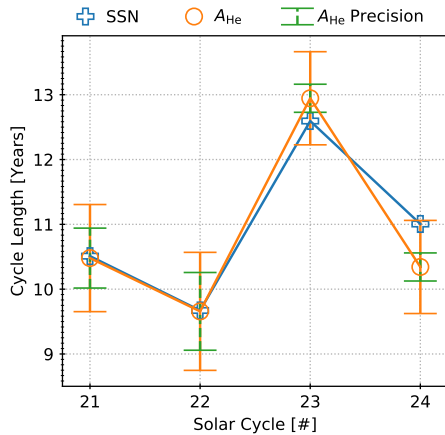


Figure 3 Blue pluses (\oplus) plot SSN cycle length as a function of cycle number as conventionally defined. Orange circles (\circ) plot the time between successive A_{He} Shutoffs as a function of the solar cycle during a given A_{He} Shutoff interval closing a Shutoff cycle occurs. This is $N - 1$ in comparison to the cycle number a given A_{He} Shutoff heralds (c.f. Figure 2). As in Figure 2's (*Left*) Panel, Orange error bars ($-$) indicates the uncertainty due to A_{He} 's precision & the 250-day averaging window. Green error bars ($--$) indicate the uncertainty due to A_{He} 's precision alone.

Figure 2 (*Left*) plots the time by which A_{He} shutoff heralds the Solar Cycle in orange circles (\circ). The uncertainty is calculated in two ways. Green error bars ($--$) indicate the uncertainty only due to A_{He} 's precision (P), i.e. the standard deviation across v_{sw} -quantiles that Figure 1 shows as blue bars. Orange error bars ($-$) show the uncertainty on A_{He} 's heralding time due to the 250-day averaging window length (W) and precision in A_{He} timing ($\sqrt{P^2 + W^2}$). The (*Right*) panel plots the (*Left*)'s uncertainty sources. Orange diamonds (\diamond) and green squares (\square) plot the uncertainties indicated in the (*Left*) panel with the corresponding color. The red dash-dotted line ($- \cdot -$) indicates the 250-day averaging window (W). This method's 250-day averaging window (Alterman and Kasper, 2019; Kasper *et al.*, 2012; McIntosh *et al.*, 2011; Kasper *et al.*, 2007) is the dominant source of uncertainty in determining when A_{He} shutoff occurs. Of note, the heralding time precision decreases starting for Solar Cycle 23 when OMNI/Lo begins transitioning to *Wind/FC* data.

Figure 3 compares SSN Cycle length (\oplus) with A_{He} shutoff cycle length (\circ), i.e. the time between consecutive A_{He} Shutoffs. SSN cycle length is plotted as a function of the conventionally defined cycle number. Shutoff cycle length is plotted as a function of the solar cycle during which the end of the Shutoff cycle interval occurs, i.e. $N - 1$ in comparison to the conventional solar cycle number a given A_{He} Shutoff heralds. A_{He} Shutoff includes the same uncertainties as Figure 2 and, again, the 250-day averaging window length is the dominant source. Excluding Cycle 24, the A_{He} shutoff cycle length is nearly identical to the SSN cycle length.

4. Brightpoints and A_{He} During the Coexistence of Two Solar Cycles

The magnetic fields underlying the Sunspot and Solar cycles extend beyond 11 years (Cliver, 2014; Srivastava *et al.*, 2018). The transition from one solar

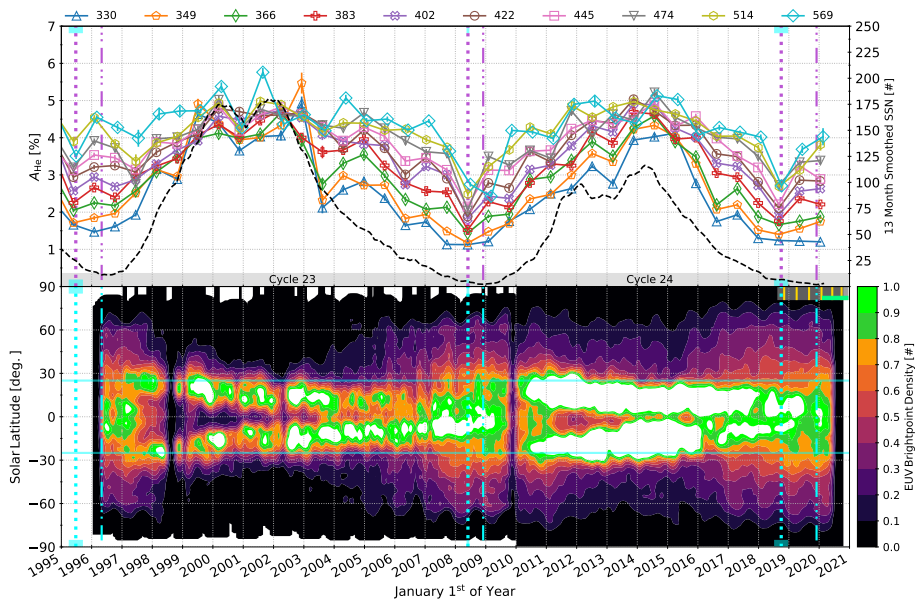


Figure 4. **(Top)** Solar wind helium abundance (A_{He}) as a function of solar wind speed (v_{sw}) and time as in Figure 1 over the time period covering 1995 to present day. **(Bottom)** A filled contour plot of the combined daily SOHO/EIT (195Å) and SDO/AIA (193Å) EUV central meridian Brightpoint (BP) density as a function of solar latitude and time. BPs are averaged down to 27 day cadence. The color scale is chosen to highlight BP density > 0.8 and levels > 1 are shown in white to emphasize BPs in the range 0.8 to 1.0. Solar Minima and A_{He} Shutoffs are plotted in light blue to contrast with BP density. Partially transparent blue lines indicate the latitudes $\lambda = \pm 25^\circ$. The gray band (■) indicates Parker Solar Probe (PSP) launch -70 days through the exit of its 6th near-Sun $+70$ days and the yellow bars (|) indicate the time spent below 0.25 AU. The green bar (■) that starts at PSP encounter 4 indicates the time period following Solar Orbiter’s (Solo) Feb 2020 launch (Müller *et al.*, 2020).

cycle to the next is not instantaneous and there is a span of time when the toroidal component of the Sun’s magnetic field exhibits polarities from both solar cycles. This is commonly seen in the overlap of adjacent solar cycles in a Butterfly diagram (Maunder, 1903; McIntosh *et al.*, 2014a; Leamon, Chapman, and Watkins, 2020; Carrington, 1863) and has contributed to the identification of an extended solar cycle (McIntosh *et al.*, 2015; Leroy and Noens, 1983; Legrand and Simon, 1981). In this context, Sunspot Minima correspond to the cancellation of oppositely signed magnetic flux from the older of the two overlapping cycles across the solar equator (McIntosh *et al.*, 2015).

Figure 4 zooms in on the time period from 1995 until present day for which SOHO and SDO provide EUV coverage. Because we are concerned with an event that happens over $\lesssim 250$ days prior to Solar Minimum, this section focuses on Solar Minima 24 and 25. We show Minimum 23 and the preceding A_{He} Shutoff for visual reference. The (*Top*) panel plots A_{He} as in Figure 1. The (*Bottom*) panel plots daily central meridian BPs averaged down to 27 day cadence. We

have applied a 1σ Gaussian filter⁹ to enhance its visual clarity. The color scale is constructed to highlight BP densities > 0.8 . Color levels > 1 are shown in white, highlighting BPs in the range 0.8 to 1. In the (*Top*) panel, Solar Minima and A_{He} 's Shutoffs are plotted as in Figure 1. In the (*Bottom*) panel, they are indicated in light blue to contrast with the BP data.

The (*Bottom*) panel also indicates the first 6 PSP near-Sun encounters and Solar Orbiter (SolO) launch in its top right corner. The gray band (■) indicates *launch* – 70 days through the exit of encounter 6 +70 days. The yellow bars (Ⓜ) indicate the time spent below 0.25 AU. The green bar (■) that starts at PSP's 4th encounter indicates the time period starting with SolO's Feb 2020 launch (Müller *et al.*, 2020). We omit A_{He} 's pre-Minimum 25 depletion date standard deviation on the top of the (*Bottom*) panel so as to not obscure the PSP encounter dates.

Comparing Figure 4's (Top) and (Bottom) panels, especially with respect to the time periods surrounding Solar Minima, is striking. Over the 4 to 5 years surrounding Solar Maxima, BPs display low levels of activity (BP Density $\lesssim 0.3$) at middle and high latitudes ($|\lambda| \gtrsim 25^\circ$). As expected (McIntosh *et al.*, 2014a), the midlatitude BPs of the emerging cycle become as or more significant than the decaying cycle prior to Solar Minima and this shift is asymmetric. For example, BP density > 0.8 appears in the northern hemisphere prior to the southern hemisphere during the time period of Minimum 24 and in the southern hemisphere before the northern hemisphere prior to Minimum 25. Comparing with A_{He} in the (Top) panel, it appears as though these asymmetric BP emergences are approximately concurrent with the depletion phase of A_{He} Shutoff to within approximately one 250-day A_{He} data point. The small size of the northern hemisphere BP emergence near the start of 2020 is a result of edge effects in the Gaussian filter. This particular feature with a BP density > 0.8 at $\lambda \gtrsim 25^\circ$ extends through to approximately the present day in the unfiltered image.

5. Discussion

Figure 1 shows that A_{He} displays the solar cycle variability characteristic of a solar activity index since at least solar cycle 21. Earlier results extend this trend back to cycles 19 and 20 (Robbins, Hundhausen, and Bame, 1970; Ogilvie and Hirshberg, 1974; Feldman *et al.*, 1978; Aellig, Lazarus, and Steinberg, 2001). Figure 1 presents an additional and as yet undiscussed feature of A_{He} 's solar cycle variation: on this 250-day timescale, A_{He} rapidly approaches and then recovers from a local minimum that departs from its long term solar cycle trends prior to Solar Minima 21 through 25. We refer to this feature as the A_{He} or Helium Shutoff.

Figure 2 (*Left*) shows that A_{He} Shutoff precedes Solar Minima by ~ 10 months. Figure 3 shows that the time between successive Shutoffs is nearly identical to the Solar Cycle concurrent with the SSN cycle for which the closing A_{He} Shutoff

⁹docs.scipy.org/doc/scipy/reference/generated/scipy.ndimage.gaussian_filter.html

Table 1. A_{He} Shutoff statistics averaged over v_{sw} -quantiles for the indicated Solar Cycles. *Heralding Time* is the time by which A_{He} Shutoff precedes the indicated Solar Minimum. A_{He} Shutoff Date is the date at which Shutoff occurred. A_{He} Shutoff precision (Prec.) is the standard deviation of the Shutoff Date. A_{He} Shutoff uncertainty = $\sqrt{P^2 + W^2}$ (Uncert.) is the geometric mean of the precision and 250-day averaging window (W). The average *Heralding Time* weighted by Shutoff Precision is 229 days and weighted by Shutoff Uncertainty is 302 days. *Cycle Length* gives the time between successive A_{He} Shutoffs for the Solar Cycle in which the A_{He} Shutoff that closes a given A_{He} Cycle occurs. A_{He} Shutoff cycle length is typically comparable to SSN cycle length.

Solar Cycle [#]	A_{He} Shutoff Date [YYYY-MM-DD]	Heralding Statistics			Cycle Length			
		Time [D]	Prec. [D]	Uncert. [D]	A_{He} Shutoff [250 D]	SSN [Y]	[250 D]	[Y]
21	1975-05-10	296	115	275	15.3	10.5	15.3	10.5
22	1985-10-29	307	232	341	14.1	9.7	14.1	9.7
23	1995-06-24	312	79	262	18.9	12.9	18.4	12.6
24	2008-05-31	184	10	250	15.1	10.3	16.1	11.0
25	2018-10-01	426	79	262	—	—	—	—

occures. Figure 2 (*Right*) shows that the largest single source of uncertainty in this analysis is the 250-day averaging windows defined by the now standard methodology we have employed (Alterman and Kasper, 2019; McIntosh *et al.*, 2011; Kasper *et al.*, 2012, 2007).

Table 1 summarizes the statistics in Figures 2 and 3. The average *Heralding Time* weighted by the inverse Shutoff Precision is 229 days and weighted by the inverse Shutoff Uncertainty is 302 days. Comparing the *Heralding Times* in Table 1, the time by which A_{He} Shutoff precedes Solar Minimum 25 is 37% larger than the next largest heralding time.

Table 1 also compares the A_{He} Shutoff and SSN Cycle lengths in units of 250 days and years, i. e. units of the 250-day averaging window and a more intuitive timescale. A_{He} Shutoff cycle 21 and 22 are identical in length to the SSN cycle. Cycles 23 are the same to within 1 averaging window. In contrast, A_{He} Shutoff cycle 24 at least a full averaging window shorter than SSN cycle 24. While the combined 362-day uncertainty¹⁰ due to the precision and averaging window length is too large to determine if this one data point is significant, that all other A_{He} Shutoffs herald SSN Minima by < 250 days and Shutoff 25 has a precision equal to Shutoff 23 suggest that Solar Minimum 25 may have occurred before the Solar Minimum 25’s recently announced^{11,12} date of December 2019. Future, higher time resolution work examine this in detail.

EUV BPs tend to form at supergranule vertices, also known as g-nodes, where the radial component of the Sun’s toroidal field emerges (McIntosh *et al.*, 2014a). They are commonly associated with the motion of giant convective cells (Hathaway, Upton, and Colegrove, 2013; McIntosh *et al.*, 2014b). Their equatorial

¹⁰ $\sqrt{79^2 + 10^2 + 2 \times 250^2}$

¹¹sidc.be/silso/node/167/#NewSolarActivity

¹²[nasa.gov/press-release/solar-cycle-25-is-here-nasa-noaa-scientists-explain-what-that-means](https://www.nasa.gov/press-release/solar-cycle-25-is-here-nasa-noaa-scientists-explain-what-that-means)

migration and torsional oscillations (McIntosh *et al.*, 2014a) along with the magnetic range of influence (MRoI¹³; McIntosh *et al.*, 2014b) with which they are associated indicate that the underlying magnetic fields have deep roots, likely in deep in the convection zone (McIntosh *et al.*, 2014b) or tachocline (McIntosh *et al.*, 2014a).

Solar magnetic activity often manifests asymmetrically: a new solar cycle typically emerges in one hemisphere before the other (McIntosh *et al.*, 2013, 2014a). Signatures of a rising cycle will also emerge before the decaying one has completely vanished. Figure 4 presents A_{He} and BPs over the time period when the necessary EIT and AIA EUV measurements are available. It indicates that, to within one 250-day A_{He} datapoint, A_{He} Shutoff occurs concurrently with or immediately prior to BP emergence in the leading hemisphere. During Solar Minimum 24, BPs emerged in the northern hemisphere before the southern. As expected (Muraközy, 2016), the southern hemisphere is now leading as we enter Solar Cycle 25.

Alterman and Kasper (2019) show that A_{He} responds to changes in SSN with a phase lag that monotonically increases with v_{sw} . Summarizing their work, slow and fast solar wind originate in distinct source regions on the Sun that are associated with distinct magnetic field strengths. Slower wind is associated with weaker magnitudes; faster wind with stronger fields. The height at which A_{He} ionizes is related to the magnetic field's strength. As such, A_{He} 's phase lag and the phase lag's v_{sw} -dependence imply that slow wind emerges from regions that are more sensitive to changes earlier in the solar cycle and these regions are associated with lower altitudes; fast wind is less sensitive to these changes and it emerges from regions associated with higher altitudes (Alterman and Kasper, 2019). Alterman and Kasper suggest that this is a signature of a filtering mechanism that reduces A_{He} from its photospheric values in a manner that depends on source region.

In contrast, A_{He} 's rapid pre-Minima depletions and then recoveries—i.e. temporary Shutoffs—occur at approximately the same time prior to Solar Minima 24 and 25 for all speeds at least as fast as 349 km s^{-1} . As such, a mechanism independent of solar wind source region and distinct from that driving the phase lag drives these Shutoffs. Given that the Shutoffs are concurrent with leading hemisphere BP midlatitude emergence (to within the 250-day averaging window) and BPs from the rising cycle emerge when two adjacent cycles overlap (McIntosh *et al.*, 2014a), we infer that these A_{He} Shutoffs are likely the result of an unique topology of the global solar magnetic field during Solar Minimum, which is driven by the equatorial cancelation of subsurface magnetic flux.

Under Parker's model, the buoyant rise of toroidal magnetic flux to the Sun's photosphere generates sunspots (Parker, 1955; Charbonneau, 2010; Cheung and Isobe, 2014). The equatorward evolution of the Sun's toroidal magnetic field component leads to the Sunspot butterfly diagram (McIntosh *et al.*, 2014a; Charbonneau, 2010; Fan, 2004). Following McIntosh *et al.* (2014a, 2015), four toroidal magnetic field bands exist during the decaying solar cycle's declining

¹³MRoI can be understood as a measure of the extent to which the solar magnetic field is open (McIntosh, Davey, and Hassler, 2006).

phases. Each hemisphere contains two bands and adjacent bands have opposite signs. These bands live for > 11 years (Cliver, 2014; Srivastava *et al.*, 2018). The poleward (rising) bands correspond to the younger of the two extended cycles; the equatorial (decaying) bands correspond to the older cycle (McIntosh *et al.*, 2014a). Solar Minima correspond to the cancelation of two older and decaying toroidal field bands at the equator. If this is the underlying mechanism, then A_{He} Shutoff could correspond to the annihilation of these two oppositely signed equatorial flux bands and corresponding lack of flux emergence.

The spacecraft providing OMNI/Lo plasma data all have orbits that are either in or close to the Earth-Sun ecliptic plane. Therefore, they may not be able to measure any helium related to the two poleward bands of the Sun’s toroidal field during these short A_{He} Shutoffs. As such, we cannot rule out the possibility that A_{He} Shutoff is due to the ecliptic nature of these spacecrafts’ orbits and this signature is not present in truly polar solar wind. Solar Oribter’s out-of-ecliptic measurements (Zouganelis *et al.*, 2020; Müller *et al.*, 2020) may help address this.

6. Conclusion

We have studied solar wind helium abundance (A_{He}) as a function of speed and time over 45 years. Using OMNI/Lo data averaged down to 250 day time resolution, we have shown that A_{He} :

- i) likely returns to a consistent values at solar cycle extrema during each of the time periods covered by Solar Minima 21 through Maximum 22 and Maximum 23 through Minimum 25;
- ii) rapidly depletes and then recovers over a time period no greater than ~ 250 days immediately prior to solar Minimum;
- iii) has recovered from its pre-Solar Minima 25 rapid depletion; and
- iv) is already increasing across v_{sw} quantiles along its solar cycle scale variability in the present day.

As solar wind from different source regions have different characteristic speeds and A_{He} at these speeds respond to solar cycle changes with a distinct phase lag (Alterman and Kasper, 2019), the concurrence of A_{He} ’s Shutoffs for speeds at least as fast as 349 km s^{-1} implies that A_{He} Shutoff is unrelated to differences in these solar wind source regions and how they generate the solar wind. That A_{He} Shutoff is approximately concurrent with the emergence of BPs in the leading hemisphere suggests that A_{He} Shutoff may be tied to the cancelation of flux from the toroidal component of solar \mathbf{B} during the time period when two adjacent solar cycles overlap, i.e. Solar Minimum. In essence, this corresponds to the death of an extended solar cycle. Therefore, A_{He} can serve as a solar activity indicator that heralds a new solar cycle’s onset before the sunspot record or other activity indicators. Although our 250-day averaging window introduces significant uncertainty into our determination of A_{He} Shutoff’s time, a comparison of the A_{He} and SSN cycles suggests that Solar Minimum 25 may have occurred prior to the recently announced December 2019.

PSP (Fox *et al.*, 2016) launched in August 2018 and first dropped below 0.25 AU on October 31st of that year. By the end of 2020, the spacecraft will have made six trips below 0.25 AU, the closest coming to within 0.2 AU of the Sun. SolO launched in February 2020 (Müller *et al.*, 2020). Figure 4 indicates PSP’s first six encounters as small yellow bars along with the time since SolO launched in light green, both in the top-right corner of the bottom panel. PSP’s 1st and 2nd near-sun encounters took place during A_{He} Shutoff. However, SolO launched after A_{He} Shutoff recovered. Based on this figure, we expect PSP—in particular SWEAP (Kasper *et al.*, 2017)—to find alpha particles become markedly more prevalent starting in Encounter 4. We also expect SolO—especially the SWA instrument suite (Owen *et al.*, 2020)—to measure an increasingly significant alpha particle abundance that does not suffer from the absence of such measurements early in the mission.

Acknowledgments This is a preprint of an article published in Solar Physics. The final authenticated version is available online at: <https://doi.org/10.1007/s11207-021-01801-9>.

The OMNI data were obtained from the GSFC/SPDF OMNIWeb interface at <https://omniweb.gsfc.nasa.gov>. NASA grants 80NSSC18K0986 and NNX17AI18G supported BLA and JCK. BLA also acknowledges NASA contract NNG10EK25C. RJL was supported by an award from the NASA Living With a Star program to NASA GSFC. SWM is supported by the National Center for Atmospheric Research, which is a major facility sponsored by the National Science Foundation under Cooperative Agreement No. 1852977.

Wind celebrated its 25th anniversary in 2019. The results presented in this paper strongly depend on the spacecraft’s long duration observations that span multiple solar cycles. As such, we wish to extend our gratitude to the teams that have and continue producing data with the instruments and the project scientists who have kept the mission running for the past quarter century.

This project made use of the following software libraries: IPython (Perez and Granger, 2007), Jupyter (Kluyver *et al.*, 2016), Matplotlib (Hunter, 2007), Numpy (van der Walt, Colbert, and Varoquaux, 2011), Pandas (McKinney, 2010), Python (Oliphant, 2007; Millman and Aivazis, 2011), HelioPy (Stansby *et al.*, 2020), IDL.

References

- Aellig, M.R., Lazarus, A.J., Steinberg, J.T.: 2001, The solar wind helium abundance: Variation with wind speed and the solar cycle. *Geophysical Research Letters* **28**(14), 2767. DOI. <http://doi.wiley.com/10.1029/2000GL012771>.
- Alterman, B.L., Kasper, J.C.: 2019, Helium Variation across Two Solar Cycles Reveals a Speed-dependent Phase Lag. *The Astrophysical Journal* **879**(1), L6. DOI. <https://iopscience.iop.org/article/10.3847/2041-8213/ab2391>.
- Alterman, B.L., Kasper, J.C., Stevens, M.L., Koval, A.: 2018, A Comparison of Alpha Particle and Proton Beam Differential Flows in Collisionally Young Solar Wind. *The Astrophysical Journal* **864**(2), 112. DOI. <http://dx.doi.org/10.3847/1538-4357/aad23f><http://stacks.iop.org/0004-637X/864/i=2/a=112?key=crossref.70d30c5e4f4e09560b242739d2b64fbc>.
- Asplund, M., Grevesse, N., Sauval, A.J., Scott, P.: 2009, The Chemical Composition of the Sun. *Annual Review of Astronomy and Astrophysics* **47**(1), 481. DOI. <http://www.annualreviews.org/doi/10.1146/annurev.astro.46.060407.145222>.
- Bachmann, K.T., White, O.R.: 1994, Observations of hysteresis in solar cycle variations among seven solar activity indicators. *Solar Physics* **150**(1-2), 347. DOI. <http://link.springer.com/10.1007/BF00712896>.
- Basu, S., Antia, H.M.: 2004, Constraining Solar Abundances Using Helioseismology. *The Astrophysical Journal* **606**(1), L85. DOI.
- Basu, S., Antia, H.M.: 2008, Helioseismology and solar abundances. *Physics Reports* **457**(5-6), 217. ISBN 0370-1573. DOI.

- Bethe, H.A.: 1939, Energy Procution in Stars. *Physical Review* **55**(1), 434.
- Bethe, H.A., Critchfield, C.L.: 1938, The formation of deuterons by proton combination. *Physical Review* **54**(4), 248. DOI.
- Carrington, R.C.: 1863, Observations of the spots on the sun from November 9, 1853, to March 24, 1861, made at Redhill, 604.
- Charbonneau, P.: 2010, Dynamo Models of the Solar Cycle. *Living Reviews in Solar Physics* **2**(1), 1. ISBN 9783642320934. DOI.
- Cheung, M.C.M., Isobe, H.: 2014, Flux emergence (Theory). *Living Reviews in Solar Physics* **11**(1). DOI.
- Cliver, E.W.: 2014, The Extended Cycle of Solar Activity and the Sun's 22-Year Magnetic Cycle. *Space Science Reviews* **186**(1-4), 169. DOI.
- Delaboudinière, J.P., Artzner, G.E., Brunaud, J., Gabriel, a.H., Hochedez, J.F., Millier, F., Song, X.Y., Au, B., Dere, K.P., Howard, R.a., Kreplin, R., Michels, D.J., Moses, J.D., Defise, J.M., Jamar, C., Rochus, P., Chauvineau, J.P., Marioge, J.P., Catura, R.C., Lemen, J.R., Shing, L., Stern, R.a., Gurman, J.B., Neupert, W.M., Maucherat, A., Clette, F., Cugnon, P., Van Dessel, E.L.: 1995, EIT: Extreme-ultraviolet Imaging Telescope for the SOHO mission. *Solar Physics* **162**, 291. DOI.
- Fan, Y.: 2004, Magnetic Fields in the Solar Convection Zone. *Living Reviews in Solar Physics* **1**(1), 1. DOI. <http://link.springer.com/10.12942/lrsp-2004-1>.
- Feldman, W.C., Asbridge, J.R., Bame, S.J., Gosling, J.T.: 1978, Long-term variations of selected solar wind properties: Imp 6, 7, and 8 results. *Journal of Geophysical Research* **83**(A5), 2177. DOI. <http://doi.wiley.com/10.1029/JA083iA05p02177>.
- Fox, N.J., Velli, M.C., Bale, S.D., Decker, R., Driesman, A., Howard, R.A., Kasper, J.C., Kinnison, J., Kusterer, M., Lario, D., Lockwood, M.K., McComas, D.J., Raouafi, N.E., Szabo, A.: 2016, The Solar Probe Plus Mission: Humanity's First Visit to Our Star. *Space Science Reviews* **204**(1-4), 7. DOI. <http://link.springer.com/10.1007/s11214-015-0211-6>.
- Hathaway, D.H.: 2015, The solar cycle. *Living Reviews in Solar Physics* **12**(1). ISBN 1614-4961. DOI.
- Hathaway, D.H., Upton, L., Colegrove, O.: 2013, Giant Convection Cells Found on the Sun. *Science* **342**(6163), 1217. DOI. <https://www.sciencemag.org/lookup/doi/10.1126/science.1244682>.
- Hirshberg, J.: 1973, Helium abundance of the Sun. *Reviews of Geophysics* **11**(1), 115. DOI. <http://doi.wiley.com/10.1029/RG011i001p00115>.
- Hunter, J.D.: 2007, Matplotlib: A 2D Graphics Environment. *Computing in Science & Engineering* **9**(3), 90. DOI. <http://ieeexplore.ieee.org/document/4160265/http://ieeexplore.ieee.org/lpdocs/epic03/wrapper.htm?arnumber=4160265>.
- Kasper, J.C., Lazarus, A.J., Steinberg, J.T., Ogilvie, K.W., Szabo, A.: 2006, Physics-based tests to identify the accuracy of solar wind ion measurements: A case study with the Wind Faraday Cups. *Journal of Geophysical Research* **111**(A3), A03105. DOI. <http://doi.wiley.com/10.1029/2005JA011442>.
- Kasper, J.C., Stevens, M.L., Lazarus, A.J., Steinberg, J.T., Ogilvie, K.W.: 2007, Solar Wind Helium Abundance as a Function of Speed and Heliographic Latitude: Variation through a Solar Cycle. *The Astrophysical Journal* **660**(1), 901. DOI. <http://stacks.iop.org/0004-637X/660/i=1/a=901>.
- Kasper, J.C., Stevens, M.L., Korreck, K.E., Maruca, B.A., Kiefer, K.K., Schwadron, N.A., Lepri, S.T.: 2012, EVOLUTION OF THE RELATIONSHIPS BETWEEN HELIUM ABUNDANCE, MINOR ION CHARGE STATE, AND SOLAR WIND SPEED OVER THE SOLAR CYCLE. *The Astrophysical Journal* **745**(2), 162. DOI. <http://stacks.iop.org/0004-637X/745/i=2/a=162?key=crossref.3243440b8824f281eaf92619ea6e90c4>.
- Kasper, J.C., Klein, K.G., Weber, T., Maksimovic, M., Zaslavsky, A., Bale, S.D., Maruca, B.A., Stevens, M.L., Case, A.W.: 2017, A Zone of Preferential Ion Heating Extends Tens of Solar Radii from the Sun. *The Astrophysical Journal* **849**(2), 126. DOI. <http://stacks.iop.org/0004-637X/849/i=2/a=126?key=crossref.a4fda357a12d19fd2ad1aa8a3897c78f>.
- King, J.H., Papitashvili, N.E.: 2005, Solar wind spatial scales in and comparisons of hourly Wind and ACE plasma and magnetic field data. *Journal of Geophysical Research* **110**(A2), A02104. DOI. <http://doi.wiley.com/10.1029/2004JA010649>.
- Kluyver, T., Ragan-kelley, B., Pérez, F., Granger, B.E., Bussonnier, M., Frederic, J., Kelley, K., Hamrick, J., Grout, J., Corlay, S., Ivanov, P., Avila, D., Abdalla, S., Willing, C.: 2016, Jupyter Notebooks—a publishing format for reproducible computational workflows. *Positioning and Power in Academic Publishing: Players, Agents and Agendas*, 87. 9781614996491. DOI.

- Laming, J.M.: 2015, The FIP and inverse FIP effects in solar and stellar coronae. *Living Reviews in Solar Physics* **12**(1). ISBN 2367-3648. DOI.
- Leamon, R.J., Chapman, W.M.S.C., Watkins, N.W.: 2020, Timing Terminators: Forecasting Sunspot Cycle 25 Onset. *Sol Phys*, 1. DOI. <http://dx.doi.org/10.1007/s11207-020-1595-3>.
- Legrand, J.P., Simon, P.A.: 1981, Ten cycles of solar and geomagnetic activity. *Solar Physics* **70**(1), 173. DOI. <http://link.springer.com/10.1007/BF00154399>.
- Leise, H., Baltzer, T., Wilson, A., Lindholm, D., Snow, M., Woodraska, D., Béland, S., Codrington, O., C., P.: 2019, LASP Interactive Solar IRradiance Datacenter (LISIRD). In: *EGU General Assembly Conference Abstracts*, European Geophysical Union, ??? <https://ui.adsabs.harvard.edu/abs/2019EGUGA..2112479L>.
- Lemen, J.R., Title, A.M., Akin, D.J., Boerner, P.F., Chou, C., Drake, J.F., Duncan, D.W., Edwards, C.G., Friedlaender, F.M., Heyman, G.F., Hurlburt, N.E., Katz, N.L., Kushner, G.D., Levay, M., Lindgren, R.W., Mathur, D.P., McFeaters, E.L., Mitchell, S., Rehse, R.A., Schrijver, C.J., Springer, L.A., Stern, R.A., Tarbell, T.D., Wuelser, J.-P., Wolfson, C.J., Yanari, C., Bookbinder, J.A., Cheimets, P.N., Caldwell, D., Deluca, E.E., Gates, R., Golub, L., Park, S., Podgorski, W.A., Bush, R.L., Scherrer, P.H., Gummie, M.A., Smith, P., Aufer, G., Jerram, P., Pool, P., Soufli, R., Windt, D.L., Beardsley, S., Clapp, M., Lang, J., Waltham, N.: 2012, The Atmospheric Imaging Assembly (AIA) on the Solar Dynamics Observatory (SDO). *Solar Physics* **275**(1-2), 17. ISBN 1120701197768. DOI. <http://link.springer.com/10.1007/s11207-011-9776-8>.
- Leroy, J.L., Noens, J.C.: 1983, Does the solar activity cycle extend over more than an 11-year period? *Astronomy & Astrophysics* **120**(2). <https://ui.adsabs.harvard.edu/abs/1983A&A...120L...1L>.
- Madjarska, M.S.: 2019, Coronal bright points. *Living Reviews in Solar Physics* **16**(1), 1. DOI. <https://doi.org/10.1007/s41116-019-0018-8>.
- Maruca, B.A., Kasper, J.C.: 2013, Improved interpretation of solar wind ion measurements via high-resolution magnetic field data. *Advances in Space Research* **52**(4), 723. DOI. <http://dx.doi.org/10.1016/j.asr.2013.04.006>.
- Maunder, E.W.: 1903, Spoerer's law of zones. *The Observatory* **26**, 329.
- McIntosh, S.W.: 2007, On the Mass and Energy Loading of Extreme-UV Bright Points. *The Astrophysical Journal* **670**(2), 1401. DOI. <http://stacks.iop.org/0004-637X/670/i=2/a=1401>.
- McIntosh, S.W., Davey, A.R., Hassler, D.M.: 2006, Simple Magnetic Flux Balance as an Indicator of Ne VIII Doppler Velocity Partitioning in an Equatorial Coronal Hole. *The Astrophysical Journal* **644**(1), L87. DOI.
- McIntosh, S.W., Kiefer, K.K., Leamon, R.J., Kasper, J.C., Stevens, M.L.: 2011, SOLAR CYCLE VARIATIONS IN THE ELEMENTAL ABUNDANCE OF HELIUM AND FRACTIONATION OF IRON IN THE FAST SOLAR WIND: INDICATORS OF AN EVOLVING ENERGETIC RELEASE OF MASS FROM THE LOWER SOLAR ATMOSPHERE. *The Astrophysical Journal* **740**(1), L23. DOI. <http://arxiv.org/abs/1109.1408><http://stacks.iop.org/2041-8205/740/i=1/a=L23?key=crossref.b41750d3c8481fd19061c8481df31ae><https://iopscience.iop.org/article/10.1088/2041-8205/740/1/L23>.
- McIntosh, S.W., Leamon, R.J., Gurman, J.B., Olive, J.-P., Cirtain, J.W., Hathaway, D.H., Burkepile, J., Miesch, M., Markel, R.S., Sitongia, L.: 2013, HEMI-SPHERIC ASYMMETRIES OF SOLAR PHOTOSPHERIC MAGNETISM: RADIATIVE, PARTICULATE, AND HELIOSPHERIC IMPACTS. *The Astrophysical Journal* **765**(2), 146. DOI. <http://stacks.iop.org/0004-637X/765/i=2/a=146?key=crossref.752f3f829a07b124b461fd9f318a0cb7>.
- McIntosh, S.W., Wang, X., Leamon, R.J., Davey, A.R., Howe, R., Krista, L.D., Malanushenko, A.V., Markel, R.S., Cirtain, J.W., Gurman, J.B., Pesnell, W.D., Thompson, M.J.: 2014a, Deciphering solar magnetic activity. I. on the relationship between the sunspot cycle and the evolution of small magnetic features. *Astrophysical Journal* **792**(1). ISBN 0004-637X. DOI.
- McIntosh, S.W., Wang, X., Leamon, R.J., Scherrer, P.H.: 2014b, IDENTIFYING POTENTIAL MARKERS OF THE SUN'S GIANT CONVECTIVE SCALE. *The Astrophysical Journal* **784**(2), L32. DOI. <https://iopscience.iop.org/article/10.1088/2041-8205/784/2/L32>.
- McIntosh, S.W., Leamon, R.J., Krista, L.D., Title, A.M., Hudson, H.S., Riley, P., Harder, J.W., Kopp, G., Snow, M., Woods, T.N., Kasper, J.C., Stevens, M.L., Ulrich, R.K.: 2015, The solar magnetic activity band interaction and instabilities that shape quasi-periodic variability. *Nature Communications* **6**, 1. ISBN 2041-1723 (Electronic)\r2041-1723 (Linking). DOI. <http://dx.doi.org/10.1038/ncomms7491>.

- Mckinney, W.: 2010, Data Structures for Statistical Computing in Python. In: van der Walt, S., Millman, J. (eds.) *Proceedings of the 9th Python in Science Conference*, 51 .
- Millman, K.J., Aivazis, M.: 2011, Python for Scientists and Engineers. *Computing in Science & Engineering* **13**(2), 9. DOI. <http://ieeexplore.ieee.org/document/5725235/>.
- Müller, D., Cyr, O.C.S., Zouganelis, I., Gilbert, H.R., Marsden, R., Nieves-Chinchilla, T.: 2020, The Solar Orbiter mission. Science overview. *Astronomy & Astrophysics* **1**, 1. DOI.
- Muraközy, J.: 2016, Phase Relationships of Solar Hemispheric Toroidal and Poloidal Cycles. *The Astrophysical Journal* **826**(2), 145. DOI. <http://dx.doi.org/10.3847/0004-637X/826/2/145>.
- Neugebauer, M.: 1981, Observations of solar-wind helium. *Fundamentals of Cosmic Physics* **7**.
- Neugebauer, M., Snyder, C.W.: 1962, Solar Plasma Experiment. *Science* **138**(3545), 1095. DOI. <http://www.sciencemag.org/cgi/doi/10.1126/science.138.3545.1095-a>.
- Ogilvie, K.W., Hirshberg, J.: 1974, The solar cycle variation of the solar wind helium abundance. *Journal of Geophysical Research-Space Physics* **79**(31), 4595. DOI.
- Ogilvie, K.W., Coplan, M.A., Bochsler, P., Geiss, J.: 1989, Solar wind observations with the ion composition instrument aboard the ISEE-3/ICE spacecraft. *Solar Physics* **124**(1), 167. DOI. <http://link.springer.com/10.1007/BF00146526>.
- Ogilvie, K.W., Chornay, D.J., Fritzenreiter, R.J., Hunsaker, F., Keller, J., Lobell, J., Miller, G., Scudder, J.D., Sittler, E.C., Torbert, R.B., Bodet, D., Needell, G., Lazarus, A.J., Steinberg, J.T., Tappan, J.H., Mavretic, A., Gergin, E.: 1995, SWE, a comprehensive plasma instrument for the WIND spacecraft. *Space Science Reviews* **71**(1-4), 55. DOI. <http://link.springer.com/10.1007/BF00751326>.
- Oliphant, T.E.: 2007, Python for Scientific Computing. *Computing in Science & Engineering* **9**(3), 10. DOI. <http://ieeexplore.ieee.org/document/4160250/>.
- Owen, C.J., Bruno, R., Livi, S., Louarn, P., Al Janabi, K., Allegrini, F., Amoros, C., Baruah, R., Barthe, A., Berthomier, M., Bordon, S., Brockley-Blatt, C., Brysbaert, C., Capuano, G., Collier, M., DeMarco, R., Fedorov, A., Ford, J., Fortunato, V., Fratter, I., Galvin, A.B., Hancock, B., Heirtzler, D., Kataria, D., Kistler, L., Lepri, S.T., Lewis, G., Loeffler, C., Marty, W., Mathon, R., Mayall, A., Mele, G., Ogasawara, K., Orlandi, M., Pacros, A., Penou, E., Persyn, S., Petiot, M., Phillips, M., Přeč, L., Raines, J.M., Reden, M., Rouillard, A.P., Rousseau, A., Rubiella, J., Seran, H., Spencer, A., Thomas, J.W., Trevino, J., Verscharen, D., Wurz, P., Alapide, A., Amoroso, L., André, N., Anekallu, C., Arciuli, V., Arnett, K.L., Ascolese, R., Bancroft, C., Bland, P., Brysch, M., Calvanese, R., Castronuovo, M., Čermák, I., Chornay, D., Clemens, S., Coker, J., Collinson, G., D'Amicis, R., Dandouras, I., Darnley, R., Davies, D., Davison, G., De Los Santos, A., Devoto, P., Dirks, G., Edlund, E., Fazakerley, A., Ferris, M., Frost, C., Fruit, G., Garat, C., Génot, V., Gibson, W., Gilbert, J.A., de Giosa, V., Gradone, S., Hailey, M., Horbury, T.S., Hunt, T., Jacquy, C., Johnson, M., Lavraud, B., Lawrenson, A., Leblanc, F., Lockhart, W., Maksimovic, M., Malpus, A., Marcucci, F., Mazelle, C., Monti, F., Myers, S., Nguyen, T., Rodriguez-Pacheco, J., Phillips, I., Popecki, M., Rees, K., Rogacki, S.A., Ruane, K., Rust, D., Salatti, M., Sauvaud, J.A., Stakhiv, M.O., Stange, J., Stubbs, T., Taylor, T., Techer, J.-D., Terrier, G., Thibodeaux, R., Urdiales, C., Varsani, A., Walsh, A.P., Watson, G., Wheeler, P., Willis, G., Wimmer-Schweingruber, R.F., Winter, B., Yardley, J., Zouganelis, I.: 2020, The Solar Orbiter Solar Wind Analyser (SWA) suite. *Astronomy & Astrophysics* **642**, A16. DOI. <https://www.aanda.org/10.1051/0004-6361/201937259>.
- Parker, E.N.: 1955, The Formation of Sunspots from the Solar Toroidal Field. *The Astrophysical Journal* **121**, 491. DOI. <http://adsabs.harvard.edu/doi/10.1086/146010>.
- Parker, E.N.: 1997, Reflections on macrophysics and the sun (Special Historical Review). *Solar Physics* **176**(2), 219. DOI.
- Perez, F., Granger, B.E.: 2007, IPython: A System for Interactive Scientific Computing. *Computing in Science & Engineering* **9**(3), 21. DOI. <http://ieeexplore.ieee.org/document/4160251/>.
- Rakowski, C.E., Laming, J.M.: 2012, on the Origin of the Slow Speed Solar Wind: Helium Abundance Variations. *The Astrophysical Journal* **754**(2011), 65. DOI.
- Robbins, D.E., Hundhausen, A.J., Bame, S.J.: 1970, Helium in the solar wind. *Journal of Geophysical Research* **75**(7), 1178. DOI. <http://doi.wiley.com/10.1029/JA075i007p01178>.
- Schwabe, H.: 1844, Sonnen — Beobachtungen im Jahre 1843. *Astronomische Nachrichten* **21**(15), 234. DOI. <http://doi.wiley.com/10.1002/asna.18440211505>.
- SILSO World Data Center: 2020, The International Sunspot Number.

- Srivastava, A.K., McIntosh, S.W., Arge, N., Banerjee, D., Dikpati, M., Dwivedi, B.N., Guhathakurta, M., Karak, B.B., Leamon, R.J., Matthew, S.K., Munoz-Jaramillo, A., Nandy, D., Norton, A., Upton, L., Chatterjee, S., Mazumder, R., Rao, Y.K., Yadav, R.: 2018, The Extended Solar Cycle: Muddying the Waters of Solar/Stellar Dynamo Modeling or Providing Crucial Observational Constraints? *Frontiers in Astronomy and Space Sciences* **5**(November), 1. DOI.
- Stansby, D., Rai, Y., Argall, M., JeffreyBroll, Haythornthwaite, R., Erwin, N., Shaw, S., Aditya, Saha, R., Mishra, S., Badger, T.G., Badman, S., Lim, P.L., Ireland, J.: 2020, heliopython/heliopy: Heliopy 0.11.1. DOI. <https://zenodo.org/record/3834844>.
- Temmer, M., Veronig, A., Hanslmeier, A.: 2003, Does solar flare activity lag behind sunspot activity? *Solar Physics* **215**(1), 111. DOI.
- Vaiana, G.S., Krieger, A.S., Timothy, A.F.: 1973, Identification and analysis of structures in the corona from X-ray photography. *Solar Physics* **32**(1), 81. DOI. <http://link.springer.com/10.1007/BF00152731>.
- van der Walt, S., Colbert, S.C., Varoquaux, G.: 2011, The NumPy Array: A Structure for Efficient Numerical Computation. *Computing in Science & Engineering* **13**(2), 22. DOI. <http://ieeexplore.ieee.org/document/5725236/>.
- Vanlommel, P., Cugnon, P., Van Der Linden, R.A.M., Berghmans, D., Clette, F.: 2005, The sidc: World data center for the sunspot index. *Solar Physics* **224**(1-2), 113. DOI.
- Zerbo, J.-L., Richardson, J.D.: 2015, The solar wind during current and past solar minima and maxima. *Journal of Geophysical Research: Space Physics* **120**(12), 250. DOI. <http://doi.wiley.com/10.1002/2015JA021407>.
- Zouganelis, I., De Groof, A., Walsh, A.P., Williams, D.R., Müller, D., St Cyr, O.C., Auchère, F., Berghmans, D., Fludra, A., Horbury, T.S., Howard, R.A., Krucker, S., Maksimovic, M., Owen, C.J., Rodríguez-Pacheco, J., Romoli, M., Solanki, S.K., Watson, C., Sanchez, L., Lefort, J., Osuna, P., Gilbert, H.R., Nieves-Chinchilla, T., Abbo, L., Alexandrova, O., Anastasiadis, A., Andretta, V., Antonucci, E., Appourchaux, T., Aran, A., Arge, C.N., Aulanier, G., Baker, D., Bale, S.D., Battaglia, M., Bellot Rubio, L., Bemporad, A., Berthomier, M., Bocchialini, K., Bonnin, X., Brun, A.S., Bruno, R., Buchlin, E., Büchner, J., Bucik, R., Carcaboso, F., Carr, R., Carrasco-Blázquez, I., Cecconi, B., Cernuda Cangas, I., Chen, C.H.K., Chitta, L.P., Chust, T., Dalmasse, K., D'Amicis, R., Da Deppo, V., De Marco, R., Dolei, S., Dolla, L., Dudok de Wit, T., van Driel-Gesztelyi, L., Eastwood, J.P., Espinosa Lara, F., Etesi, L., Fedorov, A., Félix-Redondo, F., Fineschi, S., Fleck, B., Fontaine, D., Fox, N.J., Gandorfer, A., Génot, V., Georgoulis, M.K., Gissot, S., Giunta, A., Gizon, L., Gómez-Herrero, R., Gontikakis, C., Graham, G., Green, L., Grundy, T., Haberleiter, M., Harra, L.K., Hassler, D.M., Hirzberger, J., Ho, G.C., Hurford, G., Innes, D., Issautier, K., James, A.W., Janitzek, N., Janvier, M., Jeffrey, N., Jenkins, J., Khotyaintsev, Y., Klein, K.-L., Kontar, E.P., Kontogiannis, I., Krafft, C., Krasnoselskikh, V., Kretzschmar, M., Labrosse, N., Lagg, A., Landini, F., Lavraud, B., Leon, I., Lepri, S.T., Lewis, G.R., Liewer, P., Linker, J., Livi, S., Long, D.M., Louarn, P., Malandraki, O., Maloney, S., Martinez-Pillet, V., Martinovic, M., Masson, A., Matthews, S., Matteini, L., Meyer-Vernet, N., Moraitis, K., Morton, R.J., Musset, S., Nicolaou, G., Nindos, A., O'Brien, H., Orozco Suarez, D., Owens, M., Pancrazzi, M., Papaioannou, A., Parenti, S., Pariat, E., Patsourakos, S., Perrone, D., Peter, H., Pinto, R.F., Plainaki, C., Plettemeier, D., Plunkett, S.P., Raines, J.M., Raouafi, N., Reid, H., Retino, A., Rezeau, L., Rochus, P., Rodriguez, L., Rodriguez-Garcia, L., Roth, M., Rouillard, A.P., Sahraoui, F., Sasso, C., Schou, J., Schühle, U., Sorriso-Valvo, L., Soucek, J., Spadaro, D., Stangalini, M., Stansby, D., Steller, M., Strugarek, A., Stverak, S., Susino, R., Telloni, D., Terasa, C., Teriaca, L., Toledo-Redondo, S., del Toro Iniesta, J.C., Tsiropoula, G., Tsounis, A., Tziotziou, K., Valentini, F., Vaivads, A., Vecchio, A., Velli, M., Verbeeck, C., Verdini, A., Verscharen, D., Vilmer, N., Vourlidas, A., Wicks, R., Wimmer-Schweingruber, R.F., Wiegmann, T., Young, P.R., Zhukov, A.N.: 2020, The Solar Orbiter Science Activity Plan. *Astronomy & Astrophysics* **642**, A3. DOI. <https://www.aanda.org/10.1051/0004-6361/202038445>.